Geophysical Journal International

Geophys. J. Int. (2021) **226,** 1873–1884
Advance Access publication 2021 March 31
GJI Seismology

https://doi.org/10.1093/gji/ggab122

Crustal Lg-wave attenuation in Southeast Asia and its implications for regional tectonic evolution

Yi Luo,[1,2] Lian-Feng Zhao ,[2] Zeng-Xi Ge,[1] Xiao-Bi Xie[3] and Zhen-Xing Yao[2]

[1] *School of Earth and Space Sciences, Peking University , Beijing* 100871*, China*
[2] *Key Laboratory of Earth and Planetary Physics, Institute of Geology and Geophysics, Chinese Academy of Sciences, Beijing* 100029*, China. E-mail: zhaolf@mail.iggcas.ac.cn*
[3] *Institute of Geophysics and Planetary Physics, University of California at Santa Cruz, Santa Cruz, CA* 95064*, USA*

Accepted 2021 March 29. Received 2021 March 6; in original form 2020 June 3

SUMMARY

The crustal attenuation structure can effectively reveal the rheology and thermal properties of different geological blocks, and can provide seismological constraints on regional tectonic evolution. Based on 11 306 vertical-component Lg-wave seismograms recorded at 111 broadband stations from 891 crustal earthquakes that occurred between 1994 and 2020, a broadband Lg-wave attenuation model is obtained for Southeast Asia. This study demonstrates the capability of applying crustal Lg-wave attenuation inversion in a complex region mixed with continents, islands and marginal seas. The resolution approaches 2° in most parts in the study region. Lg blockages are observed at places with sharp Moho depth changes. The resultant Q models are consistent with regional geologic structures provided by previous studies. Prominent low-attenuation anomalies are located in the Sundaland Core containing stable ancient crust, including Indochina, Malay Peninsula, East Sumatra, Sunda Shelf and Borneo Core. Regions with strong attenuation are associated with complex tectonic conditions, such as the Indo–Australian subduction zone, sutures in Sarawak and Sabah. The observed Lg-wave attenuation characteristics provide constraints on the tectonic affinities and evolutions of the geological blocks. The results show that the Borneo Core remained stable since its accretion with the Sundaland Core. Ancient blocks are characterized by weak Lg attenuation, whereas geologically younger terranes are often characterized by strong Lg attenuation, which can be exploited to better understand the separation and convergence of plates during the tectonic evolution.

Key words: Asia; Tomography; Guided waves; Seismic attenuation; Crustal structure.

1 INTRODUCTION

Southeast Asia is a tectonic convergent zone surrounded by Eurasian, Pacific and Indo–Australian plates (Fig. 1) and features continental fragments, intraoceanic island arcs, suture zones, remnants of ancient oceans and other components, forming complicated tectonic environments (Honza & Fujioka 2004; Zahirovic *et al.* 2014; Huang *et al.* 2015; Legendre *et al.* 2015). Geological studies show remarkable significances in investigating tectonic evolution in this region. However, complex terrains, widely covered sea water and jungles bring more difficulties to these studies. Seismic attenuation, as one of the important properties of the Earth, has been proved to be an effective method in studying regional geology.

At regional distances, Lg wave is the most prominent phase in seismic records. It can be considered as either summed higher mode surface waves trapped in the crustal waveguide or multiply reflected S waves supercritically bouncing between the free surface and Moho discontinuity. The amplitude of the Lg wave is very sensitive to the structure and physical properties of the waveguide. Therefore, Lg wave can provide effective constraints on the regionalization of tectonic activities down to the crustal scale (Mitchell *et al.* 1993, 1997; Zhao *et al.* 2013a; Zhao & Xie 2016; Chen & Xie 2017). Typically, Lg wave can be stably observed over the continental path, but can be completely blocked across a very short oceanic path (Zhang & Lay 1995). Beyond typical continental or oceanic crust, Lg-wave propagation can be very complicated. Some investigations reported that, on the continental shelves, Lg phase can be observed from larger earthquakes, and the data can be used for attenuation investigations over the margin area between the continent and ocean (Hong 2010; Furumura *et al.* 2014). Most of the crust in Southeast Asia has a Moho discontinuity deeper than 35 km, indicating this

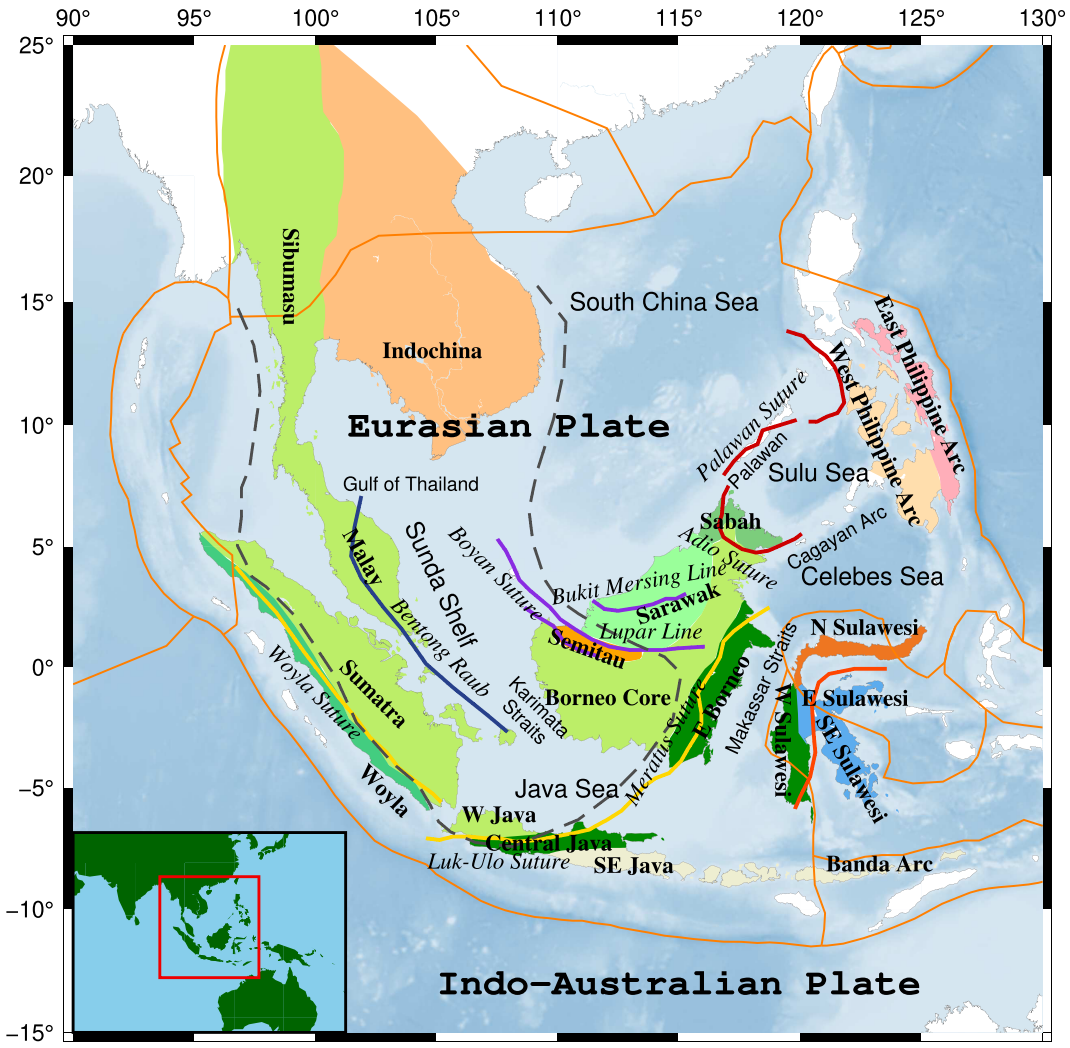

Figure 1. Map of tectonic blocks in the study region, coloured by their tectonic affinities (Hall & Wilson 2000; Zahirovic *et al.* 2014). Thin brown lines show boundaries of plates according to PB2002 (Bird 2003). Grey dashed lines show Mesozoic Sundaland Core (Hall & Wilson 2000). Bold lines are sutures (Hall & Wilson 2000; Zahirovic *et al.* 2014; Metcalfe 2017), coloured by their formation histories: blue for the closure of the Palaeo-Tethys in the Triassic (Metcalfe 2017), yellow for the closure of the Meso-Tethys in Cretaceous (Metcalfe 2017), orange for the collision between East and West Sulawesi in the Oligocene (Hall & Wilson 2000), red for the closure of the Proto-South China Sea between the Eocene and Early Miocene (Hall & Breitfeld 2017), and violet for sutures with their natures and origin times still under debate (Zahirovic *et al.* 2014; Breitfeld *et al.* 2017). Background colour shows bathymetry according to model ETOPO1 (Amante & Eakins 2009). The location of the study region is shown by the red box in the inset map.

region is characterized by the continental crust or extended shelves. This makes Lg waves able to propagate over large areas in Southeast Asia, and can be used for investigating the regional geology. Based on the above considerations, we use Lg wave to investigate crustal attenuation in Southeast Asia and explore their relations to regional geodynamics.

2 GEOLOGICAL SETTING

In Southeast Asia, several continental blocks, including Indochina, Southwest Borneo and East Java–West Sulawesi accreted with Palaeo-Asia due to the closure of different segments of the Tethys ocean at different times (Hall 2012; Yu *et al.* 2017). The Sundaland Block is composed of Myanmar, Thailand, Indochina, the Malay Peninsula, Sumatra, Java, Borneo, Palawan and the shallow-water Sunda Shelf, forming the southeastern promontory of the Eurasian Plate, and is located in the convergence zone among the Eurasian, Indo–Australian and Philippine Plates (Simons *et al.* 2007; Metcalfe 2011; Metcalfe 2017). The Sundaland Core, consisting of Sumatra, West Java, the Malay peninsula and the Sunda Shelf, separated from Gondwana in the Palaeozoic and accreted along the Eurasian margin during the Triassic and Jurassic (Hall 2012; Zahirovic *et al.* 2014). Three ancient oceans, the Paleo-Tethys (Devonian-Triassic), Meso-Tethys (Permian-Cretaceous) and Ceno-Tethys (Jurassic-Cretaceous) during the evolution of the Sundaland (Metcalfe 2017). Bentong-Raub, one of the sutures representing the remnants of the Palaeo-Tethys ocean basin, is the south part of boundary between the Sibumasu terrane in the west and the Sukhothai Arc in the east, located at the present Gulf of Thailand and Malaya. The Meratus and Luk-Ulo sutures, representing remnants of the Meso-Tethys Ocean, form the boundary between the East Java–West Sulawesi and Borneo Core (Metcalfe 2017).

Borneo, also known as Kalimantan, is the third largest island in the world with an area of ∼740 000 km^2. As a part of Sundaland, Borneo has a complex tectonic history with multiple collisions in the Mesozoic and Cenozoic (Breitfeld *et al.* 2017). Geologically, Borneo can be divided into the Borneo Core in the southwest, Sarawak in the northwest, Sabah in the northeast and east Borneo. The Borneo Core, lying to the south of the Lupar suture (Fig. 1), forms the southeastern corner of the Sundaland continental promontory (Yang & Peng 2004). The northern part of the Borneo Core (western Kuching Zone) is interpreted to belong to the Mesozoic eastern Sundaland margin (Breitfeld *et al.* 2017) and has the oldest strata, including the Devonian to the Jurassic (Yan 2005). Northern Borneo, including Sarawak and Sabah, is the northern part of the Sundaland continental margin and records collisions between Sundaland and microcontinental fragments (Hall & Wilson 2000) and subductions of several ancient oceans (Hall & Breitfeld 2017). The Rajang Accretionary Complex in Sarawak and central Sabah, northwestern Borneo, is a thick accretionary complex resulted from the Eocene bending of Borneo (Hutchison 1996; Honza & Fujioka 2004). Sulawesi is a region of Cenozoic collision between continental, ophiolites and island arc fragments (Hall & Wilson 2000). West Sulawesi represents the margin of the Eurasian Plate, which was a subduction-related volcanic arc during the Palaeogene, and accreted to the Borneo Core in the Late Cretaceous (Zahirovic *et al.* 2014). The eastern part of Sulawesi (fragments of the Australian continental margin) collided with the West Sulawesi at approximately 25 Ma, causing many tectonic events in both Sulawesi and Borneo (Hall & Wilson 2000).

3 DATA AND METHOD

3.1 Data and pre-processing

Seismic data were collected from 891 crustal earthquakes between 1994 and 2020 recorded by 111 broad-band seismic stations in Southeast Asia. Because the study area has both oceanic and continental environments, Lg-wave energy decays faster than it does in a typical continental crust. To ensure a good signal-to-noise ratio (SNR), we selected events of magnitudes ranging from 5.2 to 7.4, larger than typical magnitude range used in previous Lg-wave studies. For these larger events, their rupture processes on Lg wave amplitudes are neglected. To guarantee all sources are crustal events, only those with their depths shallower than either the local Moho depth or regional averaged Moho depth (25 km) were used. The epicentral distances are between 200 km and 3000 km, in which clear Lg waveforms can be observed. Only events recorded by at least three stations, and stations recorded at least three events were used. Fig. 2 shows the distributions of events and stations used in this study (for details see Tables S1, S2 and S3 in supplementary data).

The data pre-processing procedure followed previous studies (Zhao *et al.* 2010, 2013a,b). For the Lg amplitude measurement, we selected the most energetic waveforms within a group velocity window between 3.0 and 3.6 km s^{-1}, a typical range for Lg-wave observations. Meanwhile, the noises were used for both data quality control and correcting the Lg-wave amplitudes. Both pre-event noise and pre-phase noise have been considered by different authors for the above purposes (e.g. Xie *et al.* 2004; Phillips *et al.* 2005; Pasyanos *et al.* 2009; Zhao *et al.* 2010, 2013a; Chen & Xie 2017). The background (pre-P) noise usually can be considered as a stable random series. It is expected that its amplitude in the Lg-wave window can be properly predicted from the measurement in pre-P time window. However, the coda waves from the *P* and *Sn* waves can also enter the Lg-wave window, often causing more serious effect on the Lg-wave measurement than the background noise. On the other hand, these coda waves are scattered waves, instead of stable phases. Their amplitudes decay with elapsed times and strongly depend on the frequency. Using the pre-phase coda amplitudes to predict the amplitudes in the Lg window, a frequency-dependent coda decay model is required. Otherwise, the process may introduce additional errors. Considering the complexity of the research area, we used both pre-event and pre-phase noise to select the obtained Lg-wave spectra.

We used a time window, which has the same length as the Lg-wave window, before the first-arriving *P* wave to extract the pre-event ambient noise. The SNR can be calculated as

$$\mathrm{SNR}(f) = A_{\mathrm{Origin}}(f)/A_{\mathrm{Noise}}(f), \tag{1}$$

where $A_{\mathrm{Origin}}(f)$ and $A_{\mathrm{Noise}}(f)$ are power spectra of the raw Lg wave and noise series, respectively. Lg-wave data with SNR(f) lower than a threshold of 2.0 were considered as low quality and automatically discarded from the data set.

The pre-phase noise was retrieved using a similar window right before the Lg-wave arrival. Referred to Furumura *et al.* (2014), the records with pre-phase SNR lower than 1.0 were considered having very weak or no Lg signal. Due to its complexity, the pre-phase noise was not adopted in the correction of Lg-wave spectrum.

Then, the power spectrum of the Lg-wave signal can be obtained as

$$A^2_{\mathrm{Lg}}(f) = A^2_{\mathrm{Origin}}(f) - A^2_{\mathrm{Noise}}(f). \tag{2}$$

After the pre-processing, a total of 11 306 vertical-component Lg-wave spectra were obtained. Regional waveforms from two typical earthquakes are presented in Figs 3 and 4. The Lg phases can be clearly observed through propagation paths mainly crossing continental crust, for example from KOM to NAYO in Fig. 3 and from CMAI to NONG in Fig. 4. For paths mixed with continental shelf and shallow water, the Lg waves show reduced amplitudes and longer durations, for example PSI, KAPI and PRAC in Fig. 3. For paths crossing oceanic crust, Lg phases were hardly observed, for example stations in southeast China, Philippine and Indian Ocean. The thinning crust and sea water eliminate Lg signal by extracting Lg energy to the mantle and sea water and elongating the Lg wave train (Furumura *et al.* 2014). Scattering caused by complex structures may also be responsible for longer Lg-wave trains and lower Lg amplitudes. Only records that meet both pre-event and pre-phase SNR thresholds are considered for inversion.

3.2 Modelling of the Lg-wave spectrum

The spectral amplitude $A(f)$ of the Lg wave can be described as (Xie & Mitchell 1990)

$$A(f) = S(f)(\Delta_0\Delta)^{-\frac{1}{2}} \cdot \exp\left[-\frac{\pi f}{V}\cdot\int_{\mathrm{ray}}\frac{\mathrm{d}s}{Q(x,y,f)}\right]X(f), \tag{3}$$

where $S(f)$ represents the source spectrum, Δ is the epicentral distance, Δ_0 is a reference distance set to be 100 km (Street *et al.* 1975; Herrmann & Kijko 1983; Zhao *et al.* 2018), V represents the Lg-wave group velocity, $Q(x, y, f)$ is the frequency-dependent Lg-wave quality factor which is a function of frequency f and location (x, y) on a ray path, $X(f)$ is the frequency-dependent site response function.

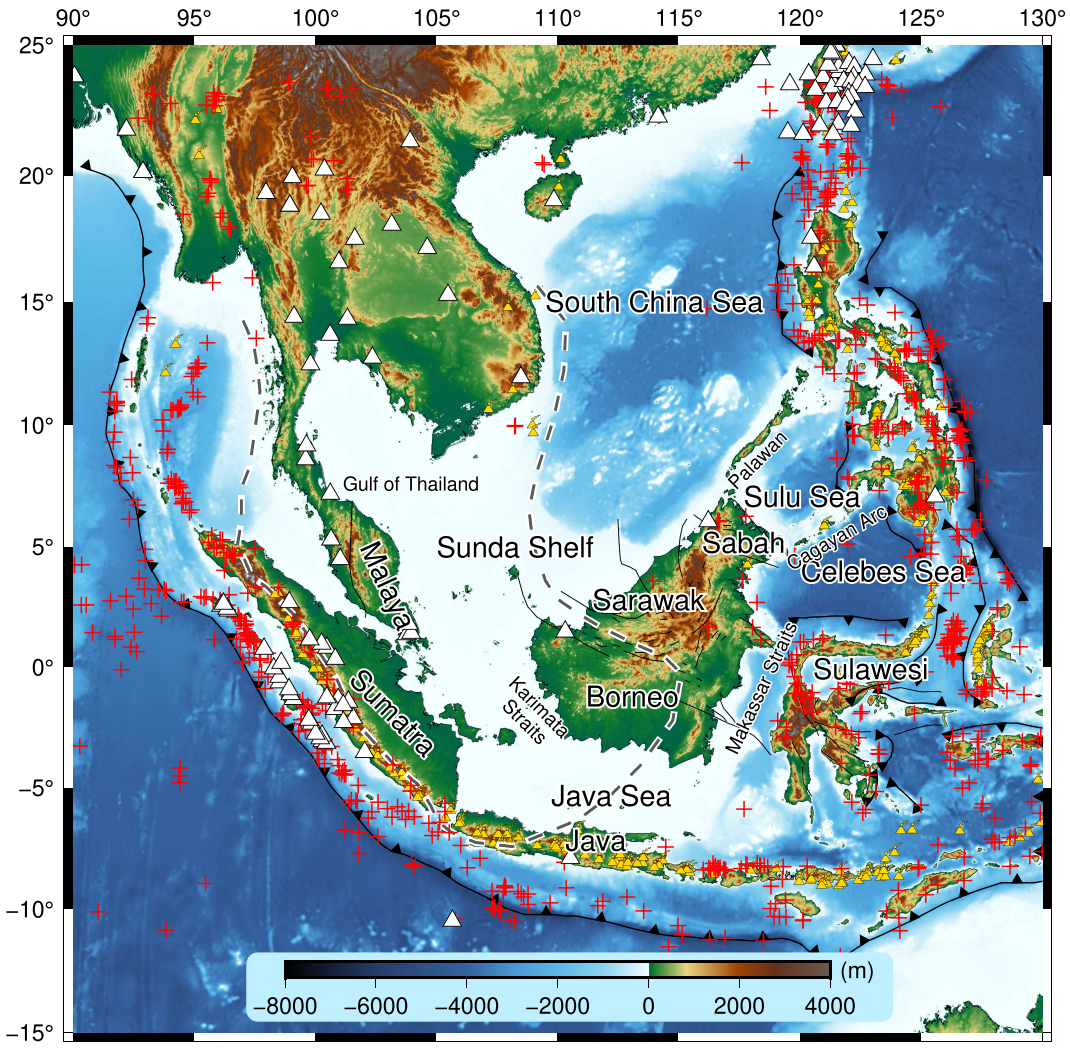

Figure 2. Distributions of earthquakes (red crosses) and seismic stations (white triangles) used in the Q estimation. Thick black lines with teeth show boundaries of plates according to PB2002 (Bird 2003). Thin black lines are major faults (Hall 1996; Hall & Wilson 2000; Yan 2005; Chan *et al.* 2017). Active volcanoes are also shown as gold triangles with plumes (Global Volcanism Program 2013). Background colour shows the topography and bathymetry according to model ETOPO1 (Amante & Eakins 2009).

The Lg-wave excitation function $S(f)$ can be expressed as (Street *et al.* 1975)

$$S(f) = \frac{M_0 R}{4\pi\rho v_s^3} \cdot \frac{1}{1+(f/f_c)^2}, \tag{4}$$

where M_0 is the scalar seismic moment, f_c is the source corner frequency, R is the radiation pattern, and ρ and v_s are the density and shear wave speed in the near source region, respectively. For events with moderate magnitude, the Lg-wave radiation pattern can be assumed unity (Zhao *et al.* 2018).

When we have Lg-wave records at two stations i and j from the same event k, and the locations of the two stations are approximately on the same great circle from the epicentre, the source spectrum can be eliminated from the two-station spectral ratio as

$$A_{ij} = \frac{A_{kj}}{A_{ki}} = \left(\frac{\Delta_{kj}}{\Delta_{ki}}\right)^{-\frac{1}{2}} \cdot \exp\left[-\frac{\pi f}{V} \cdot \int_i^j \frac{\mathrm{d}s}{Q(x,y,f)}\right] \cdot \frac{X_j}{X_i}, \tag{5}$$

where A_{ij} represents the two-station spectral ratio between observed amplitudes A_{kj} at station j and A_{ki} at station i from earthquake k, Δ_{kj} and Δ_{ki} are epicentral distances from earthquake k to stations j and i, respectively, X_j and X_i are the site responses at stations j and i, respectively. Eqs (3) and (5) form the single-station and two-station data sets, which can be further used in Lg-wave attenuation inversion (Xie & Mitchell 1990; Xie 1993). The single-station method provides better area coverage because each event–station pair can independently constrain the Q along the great circle path. However, the trade-off between the source term and attenuation in eq. (3) may cause crosstalk which introduces ambiguities in the inversion. The two-station data in eq. (5) can automatically eliminate the source term from observations, leading to measurements free of source effect. However, the two-station data require the source and two stations located on the same great circle, and the effective ray path shrinks to path between the two stations. These largely limited the available two station data set. Furthermore, the two-station ray path is far away from the source, where the SNR tends to be considerably lower than single station data. This further reduces the actual

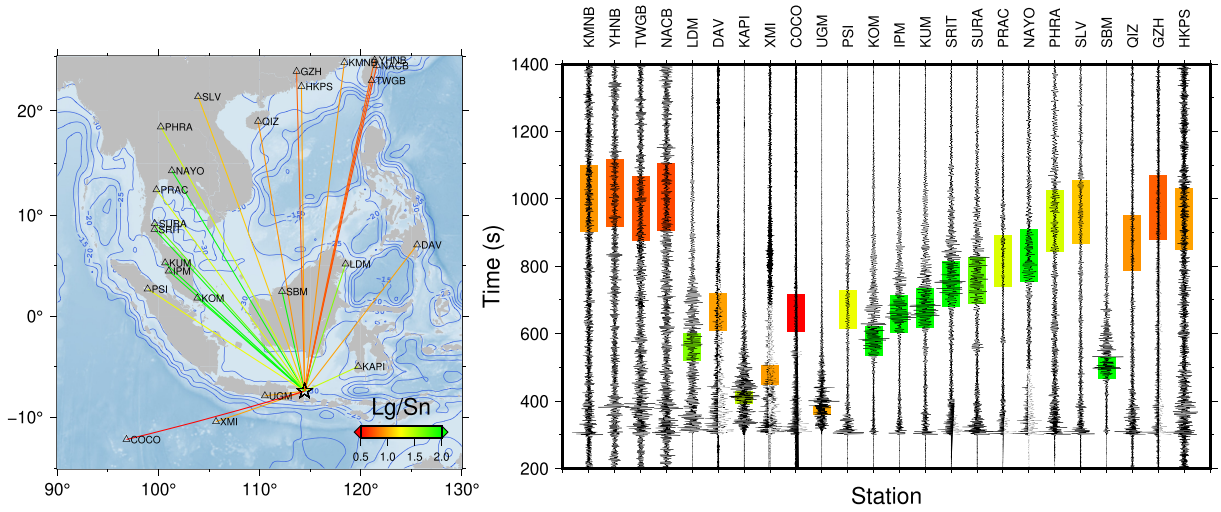

Figure 3. Normalized vertical-component velocity seismograms from a crustal earthquake occurred on 2018 October 10 with magnitude of M_w 6.0. The propagation paths are colour coded by their pre-phase SNR. Blue contours show Moho depth based on the CRUST1.0 model (Laske *et al.* 2013). Background colour shows bathymetry according to model ETOPO1 (Amante & Eakins 2009). The waveforms are filtered with a passband between 0.5 and 3.0 Hz, aligned at the arrival time of *P* phase and ordered according to their azimuth.

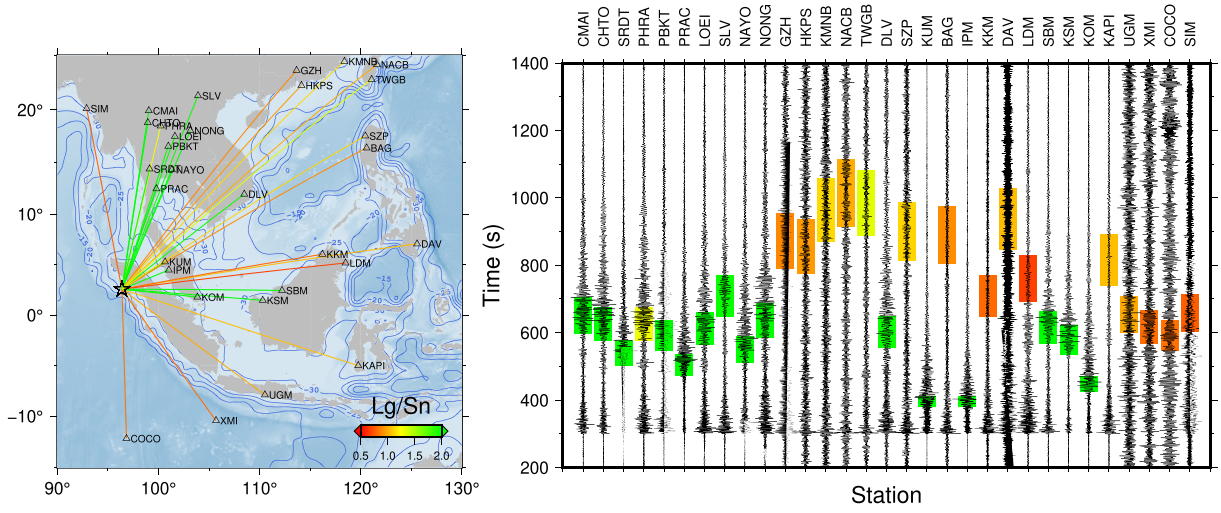

Figure 4. Similar to Fig. 3, but for an earthquake occurred on 2011 January 18 with a magnitude of M_w 6.0.

coverage of the two-station data. In this study, we jointly used both single- and two-station data in consideration of both precision and path coverage.

3.3 Lg-wave *Q* inversion

Taking the natural logarithms on both sides of eq. (3) and assuming that $r\,(f) = 1$, we have

$$\ln[A(f)] = \ln[S(f)] + \ln\left[(\Delta_0\Delta)^{-\frac{1}{2}}\right] - \frac{\pi f}{V} \times \int_{\text{ray}} \frac{\mathrm{d}s}{Q(x,y,f)} + \ln[X(f)]. \quad (6)$$

The terms $Q(x, y, f)$, $\ln[S(f)]$ and $\ln[X(f)]$ can be expressed in perturbation forms as

$$\frac{1}{Q(x,y,f)} \approx \frac{1}{Q^0(x,y,f)} - \frac{\delta Q(x,y,f)}{\left[Q^0(x,y,f)\right]^2}, \quad (7)$$

$$\ln[S(f)] = \ln\left[S^0(f)\right] + \delta\ln[S(f)], \quad (8)$$

$$\ln[X(f)] = \ln\left[X^0(f)\right] + \delta\ln[X(f)], \quad (9)$$

where S^0, Q^0 and X^0 represent the initial values of source spectrum, Q value and site response spectrum for starting the inversion. Then we obtain

$$\tilde{h} = \sum_{m=1}^{M}[a_m \cdot \delta\ln Q_m] + \delta(\ln S) + \delta(\ln X), \quad (10)$$

where we discretized the integral over the Lg-wave ray path into summation over model elements. The total number of model elements involved in a ray path is M, and the coefficient a_m is related to the length of the ray segment at mth element. $\tilde{h}$ is the residual between the observed and synthetic Lg-wave spectra and can be expressed as

$$\tilde{h} = \ln[A(f)] - \ln\left[S^0(f)\right] - \ln[G(\Delta)] + \frac{\pi f}{V} \times \int_{ray} \frac{\mathrm{d}s}{Q^0(x,y,f)} - \ln\left[X^0(f)\right]. \quad (11)$$

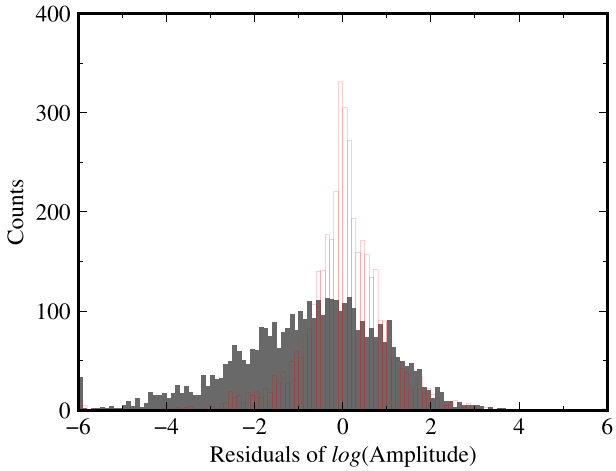

Figure 5. Distribution of 1.0 Hz residuals before (grey) and after (red) the inversion.

Gathering all the single-station measurements, we derive the matrix equation for the perturbation of the Q model as

$$\boldsymbol{H}_{\rm SSM} = \boldsymbol{A}_{\rm SSM} \cdot \delta \boldsymbol{Q} + \delta \boldsymbol{S} + \delta \boldsymbol{X}. \quad (12)$$

For two-station measurements, the source term is eliminated, and the matrix equation becomes

$$\boldsymbol{H}_{\rm TSM} = \boldsymbol{A}_{\rm TSM} \cdot \delta \boldsymbol{Q} + \delta \boldsymbol{X}. \quad (13)$$

Combining the single- and two-station measurements, we have

$$\begin{bmatrix} \boldsymbol{H}_{\rm SSM} \\ \boldsymbol{H}_{\rm TSM} \end{bmatrix} = \begin{bmatrix} \boldsymbol{A}_{\rm SSM} \\ \boldsymbol{A}_{\rm TSM} \end{bmatrix} \cdot \delta \boldsymbol{Q} + \begin{bmatrix} 1 \\ 0 \end{bmatrix} \cdot \delta \boldsymbol{S} + \delta \boldsymbol{X}. \quad (14)$$

The above equation forms an inversion problem for unknown vectors $\delta \boldsymbol{Q}$, $\delta \boldsymbol{S}$ and $\delta \boldsymbol{X}$, and can be solved by the least-squares QR method (Paige & Saunders 1982). For the initial model, we use the low-resolution regional average result obtained from the two-station data (Zhao *et al.* 2010). As an example, illustrated in Fig. 5 are distributions of 1.0 Hz residuals before and after the inversion. We see that, after the inversion, the distribution tended to be Gaussian shaped with a zero mean and a much smaller standard deviation.

4 RESULTS

Tomographic inversions were conducted for the Lg-wave Q values at 58 frequencies from 0.05 to 10.0 Hz with an increment of 0.04 on the base 10 logarithm scale. The resulting $Q_{\rm Lg}$ variation maps at three selected frequencies at 0.2, 1.0 and 2.0 Hz are shown in Fig. 6, along with the corresponding checkerboard resolution tests and ray path distributions. Overall, the regional $Q_{\rm Lg}$ increases with increasing frequencies. In most land areas, e.g. Indochina, Borneo, Sumatra and Java, the spatial resolution can reach approximately $2^\circ \times 2^\circ$. However, due to the sparse path coverage, the spatial resolutions in the Gulf of Thailand, South China Sea and Sulawesi are relatively poor. Due to the highly uneven distribution of stations, available ray paths of two-station measurements are very limited and mainly cover Indochina and Sumatra. The high-frequency Lg signal tends to be strongly attenuated both due to the intrinsic and scattering mechanisms, resulting in substantial loss of data due to low SNR. Therefore, at high frequencies, the ray coverage is considerably sparser than that at low frequencies.

To investigate the Lg-wave attenuations in different tectonic environments, we compared $Q_{\rm Lg}$ values averaged in different regions and at different frequencies in the study region. The regional average is calculated over inverted Q values of all cells in that region. The Q value at a nominal frequency is calculated by directly average the logarithmic Q within a narrow frequency range neighboring that frequency. It can be seen in Fig. 7 that regions including the Karimata Straits and Java Sea do not block the Lg-wave propagation even they are covered by shallow sea water, mainly because Sundaland is composed of a typical continental crust with a deep Moho discontinuity. In addition, as shown in Fig. 2, seismic activity is relatively low in Sundaland. Cold and stable ancient crust is characterized by relatively low attenuation. In contrast, Q values decrease significantly at plate boundaries, sutures, orogenies, basins with thick sediments and oceanic fragments. Structures with complex tectonic evolution history tend to exhibit strong attenuation. The Indian Ocean southwest of Sumatra and the Banda Sea east of Sulawesi also have low-Q values as the Lg wave decays significantly in the oceanic crust (Zhang & Lay 1995).

Fig. 8 illustrates the average $Q_{\rm Lg}$ versus the frequency for five main blocks in the study region. The frequency-dependent $Q_{\rm Lg}$ can be further investigated in two subfrequency bands: 0.05–1.0 and 1.0–10.0 Hz. Within each band, a band limited power-law $Q_{\rm Lg}$ model

$$Q_{\rm Lg} = Q_0 \, f^{\eta} \quad (15)$$

can be obtained using linear regression, where Q_0 and η are constants for individual blocks and frequency bands.

The average $Q_{\rm Lg}$ values shown in Fig. 8(f) indicate that, in the 0.2–3.0 Hz frequency band, the five major tectonic blocks in Southeast Asia show different behaviours in Lg-wave attenuation, including their Q values and frequency dependences. The Malay Peninsula shows the highest $Q_{\rm Lg}$ (anomaly coded #1 in Figs 6, 7 and 9), which characterizes an ancient and stable block like the Eurasian Plate. In contrast, Sumatra and Borneo appear to have the lowest Lg Q.

5 DISCUSSIONS

We investigate lateral variations of the frequency-dependent $Q_{\rm Lg}$ along five profiles crossing regions with strong Lg-wave attenuations linked to sutures and boundaries of tectonic blocks.

5.1 The Sundaland Core

From profiles A and B in Figs 9(b) and (c), we see clearly the shape of the Sundaland Core associated with high-Q anomalies (coded #1). Cold and stable ancient crust has a relatively weak attenuation. The Bentong-Raub suture, the remnant of the Palaeo-Tethys ocean basin, cannot be clearly identified as a fragile zone, possibly because subduction occurred in the middle-late Triassic and, during the evolution, the two parts have been closely integrated into one. By studying the effective elastic lithosphere thickness, Shi *et al.* (2017) indicated that the Borneo Core and the Singapore platform might belong to the same block because they share similar strength features. High-Q zones in 105°E–110°E along profile A, 105°E–116°E on profile B and 100°E along profile C are consistent with the Sunda Shelf and Borneo Core, indicating that the Borneo Core has a similar long accretion history with the Malay Peninsula and East Sumatra. The Sundaland Core has remained stable since it formed, despite the prominent tectonic evolution in

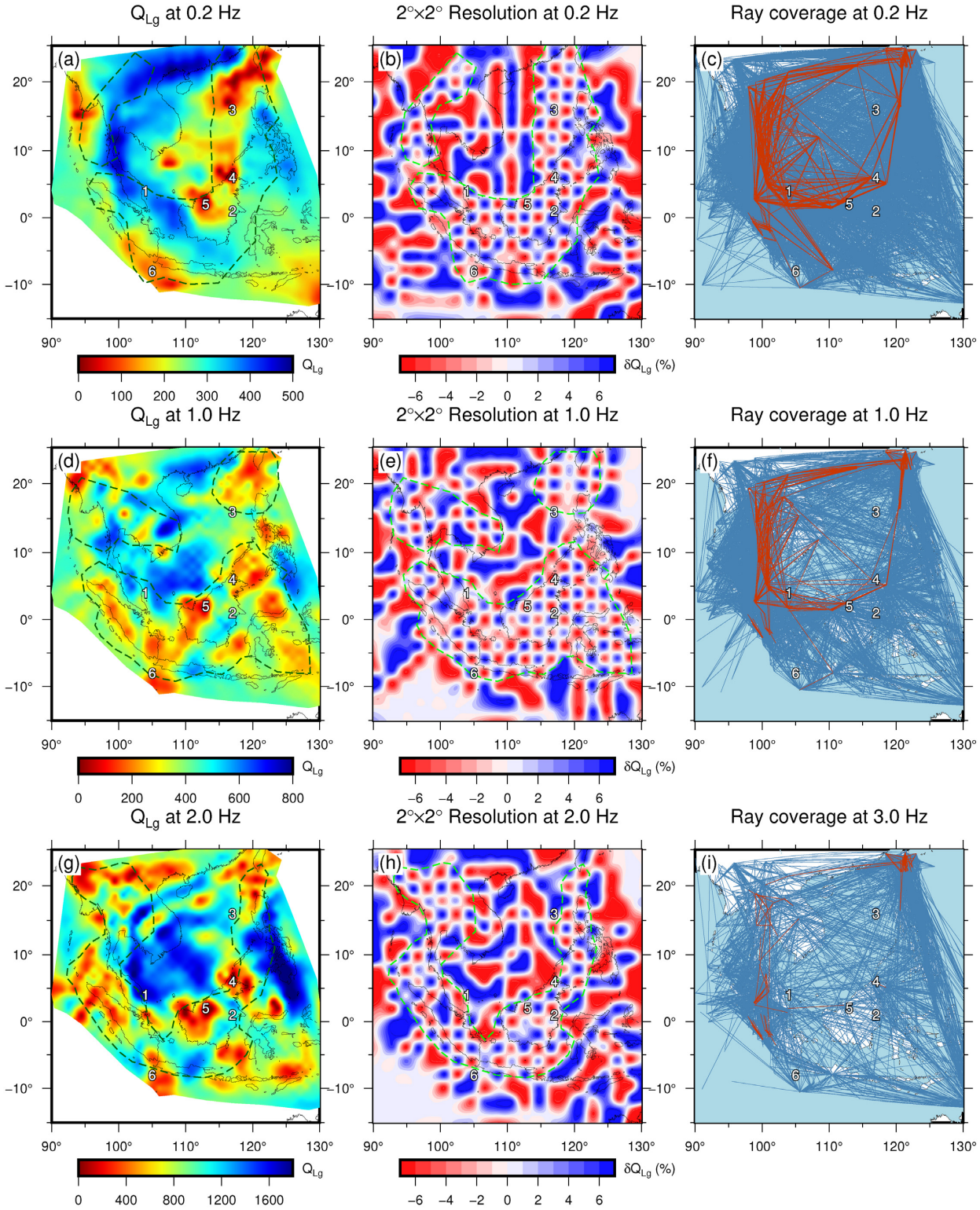

Figure 6. Lateral variation in Q_{Lg} (left), resolution test (middle) and associated ray path coverage (right) at 0.2 Hz (a–c), 1.0 Hz (d–f) and 3.0 Hz (g–i). Dashed lines in left and middle panels show sites with adequate resolutions. Different colour scales are used for different frequencies. In ray coverage maps, blue and red lines indicate paths for single- and two-station measurements, respectively. Black lines are coast lines. The code numbers indicate regions' Q_{Lg} anomalies.

Southeast Asia. In profile D in Fig. 9(e), from 98°E to 110°E, the Sunda Shelf shows low attenuation over a wide frequency band. From 110°E to 113°E, Q is slightly lower but still higher than in the volcanic island arc in the southeast. In profile D, a clear change in Q_{Lg} between 0.3 and 1.5 Hz can be seen at 110°E, where the Luk-Ulo and Meratus Sutures are considered to be the southern boundary of the Sundaland Core (Zahirovic *et al.* 2014; Metcalfe 2017). Advokaat *et al.* (2018) suggested that the distributed

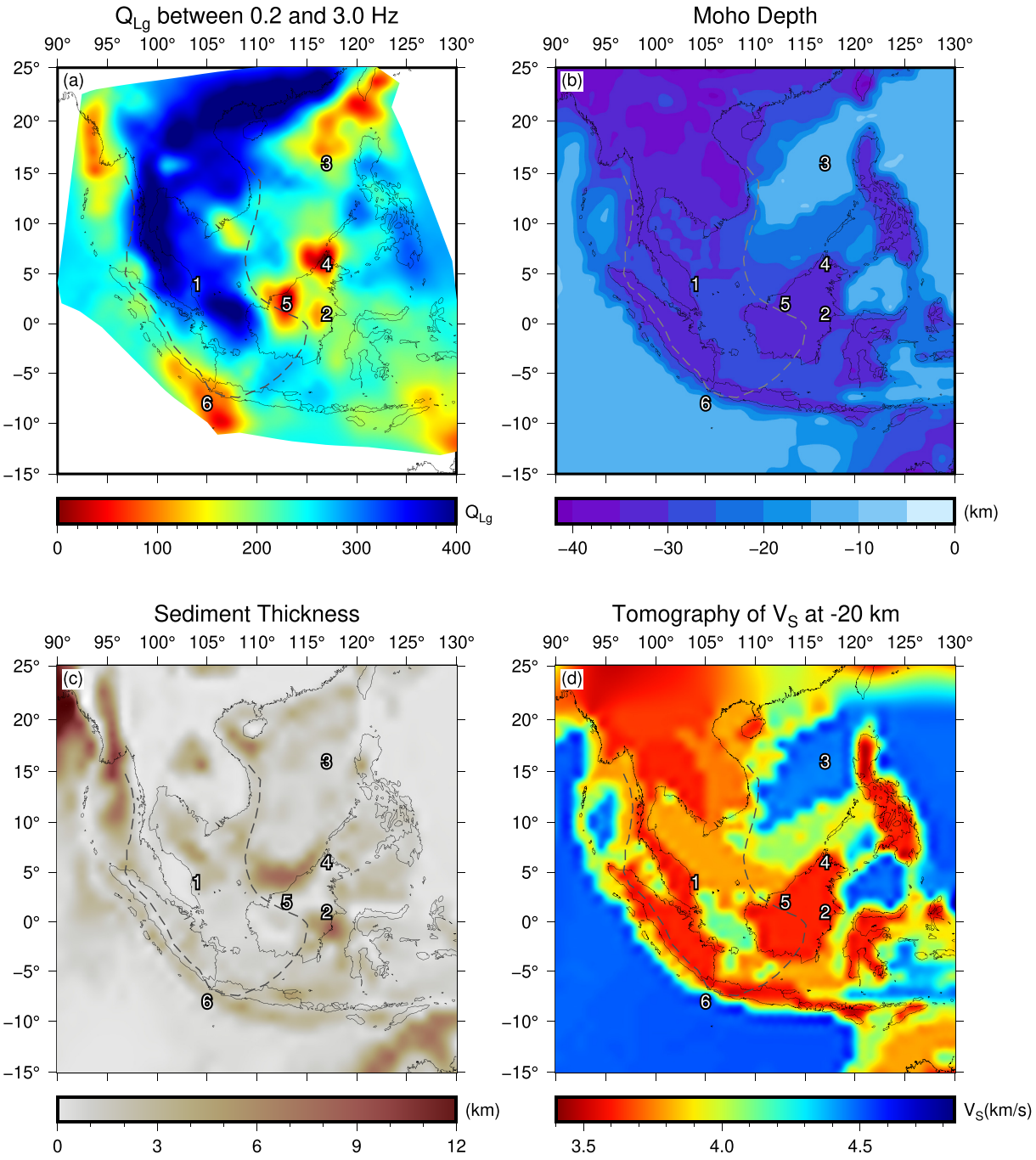

Figure 7. Maps of (a) Q_{Lg} averaged over the 0.2–3.0 Hz band and under the logarithmic scale, (b) Moho depth, (c) sediment thickness and (d) thickness-weighted average V_s in the crust based on the CRUST1.0 model (Laske *et al.* 2013).

extension in the West Java Sea between Borneo and Sumatra is related to the rotation of Borneo in the Cenozoic. Therefore, the crustal thinning and strong tectonic activities may contribute to the low-Q anomaly.

Fig. 9(b) shows that, in profile A, there are high shear wave velocity anomalies below the crust under the Sunda Shelf (105°E–110°E) and the Sulu Sea (119°E–123°E). However, the Sulu Sea shows stronger attenuation than the Sunda Shelf at low frequencies, which may result from relatively thinner oceanic crust (Zhang & Lay 1995). Additionally, the age of the oceanic lithosphere of the Sulu Sea is relatively young (Müller *et al.* 2008; Huang *et al.* 2015), indicating that it has an unstable crust. Therefore, the Sulu Sea is characterized by low Q_{Lg} at low frequencies. In contrast, at frequencies above 2 Hz, the Sulu Sea has a relatively high-Q value which may result from that the oceanic crust can hold more overtones and allow the high-frequency Lg wave to develop (Zhang & Lay 1995).

5.2 Collisions between the Borneo Core and East Java–West Sulawesi

The similar high-Q characteristics shared by West Sulawesi and east Borneo may imply their similar origins. Metcalfe (2017) suggested

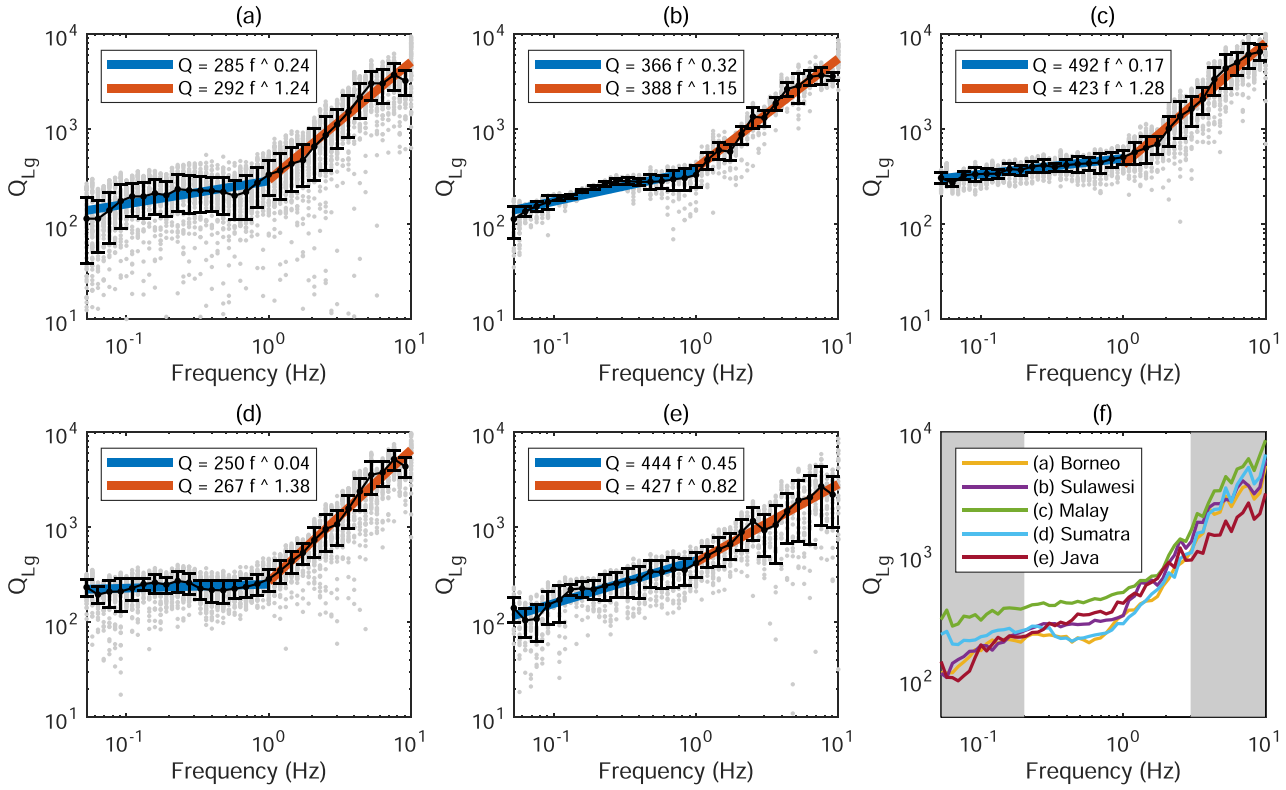

Figure 8. Frequency dependence of the average Q_{Lg} in five tectonic blocks including (a) Borneo, (b) Sulawesi, (c) the Malay Peninsula, (d) Sumatra and (e) Java. Grey dots are inverted Q_{Lg} values from individual model cells, while black dots and error bars are averaged values and standard deviations within the tectonic blocks and frequency intervals. Power-law Q_{Lg} models at different frequency bands are plotted with coloured lines. (f) Comparison of the frequency-dependent average Q_{Lg} in all five blocks, where the white region highlights the 0.2–3.0 Hz frequency band.

that East Java–West Sulawesi and southwest Borneo were separated from northwest Australia in the Jurassic and accreted to the Sundaland in the Cretaceous, during the closure of the Meso-Tethys Ocean. Anomalies coded #2, located between 116°E and 120°E along Profile B (Fig. 9) is the eastern extension of the Meratus Suture, which is considered to be the boundary between the Borneo Core and southeast Borneo. The low-Q anomaly appears in a frequency band around 0.5–1.0 Hz along profiles B and D. Strong frequency dependence may indicate plausible scattering attenuation but need more evidence for this point.

5.3 Sutures in Sabah, Cagayan Arc and Palawan

The Proto-South China Sea was an ancient ocean located between South China and Borneo. When the South China Sea began to expand, the Proto-South China Sea subducted southeastwards beneath Sabah and Cagayan between the Eocene and Early Miocene (Hall & Breitfeld 2017). Near 117°E in Profile A, there is a low-Q anomaly (coded #4), which could be associated with sutures in Sabah (Fig. 1). The subduction of the Proto-South China Sea left traces along Sabah and the Cagayan Arc, which is outlined by low-Q anomalies in Figs 6 and 7. The Palawan block, along with several microcontinental segments on the northern margin of Borneo, detached from South China and accreted to Borneo during the expansion of the South China Sea. The low-Q anomaly can be observed along Palawan Island at low frequencies. Additionally, the study by Hall & Breitfeld (2017) suggested that the Palawan Trough is not the subduction trench of the Proto-South China Sea, instead, it represents a continent–ocean transition at the southeastern edge of the South China Sea. For a subduction trench, the Lg waves usually decay strongly, whereas a continent–ocean transition or a continental shelf extension area is characterized by relatively weak attenuation, such as observed low-Q_{Lg} anomalies in the Sumatra and high-Q_{Lg} values in the Sunda shelf. We observed high Q_{Lg} in the Palawan Trough, which may support that the Palawan Trough is a continent–ocean transition at the southeastern edge of the South China Sea (Hall & Breitfeld 2017).

5.4 Sutures in Sarawak

Several studies have suggested that the accretion of northern Borneo occurred in the Cenozoic and was affected by the subduction of the Proto-South China Sea. The Semitau Block, a Cathaysian terrane from South China, is sandwiched between the Lupar Line and the Boyan Suture and accreted to northern Borneo in the mid-Eocene, resulting in the Sarawak Orogeny (Zahirovic *et al.* 2014; Metcalfe 2017).

In our result, near 113°E in profiles A and E, a prominent low-Q anomaly (coded #5) can be associated with Semitau and three sutures sandwiching it. According to the upper-mantle S-wave velocity tomography by Lebedev & Nolet (2003), low-velocity anomalies beneath Sarawak at the depth of 60 and 100 km correlate well with both the location of the suture zone and the low-Q anomaly in our result. The low-Q anomaly in the crust and the low-velocity anomaly in the upper mantle may jointly indicate a much active tectonic area in Sarawak. According to Zahirovic *et al.* (2014) and

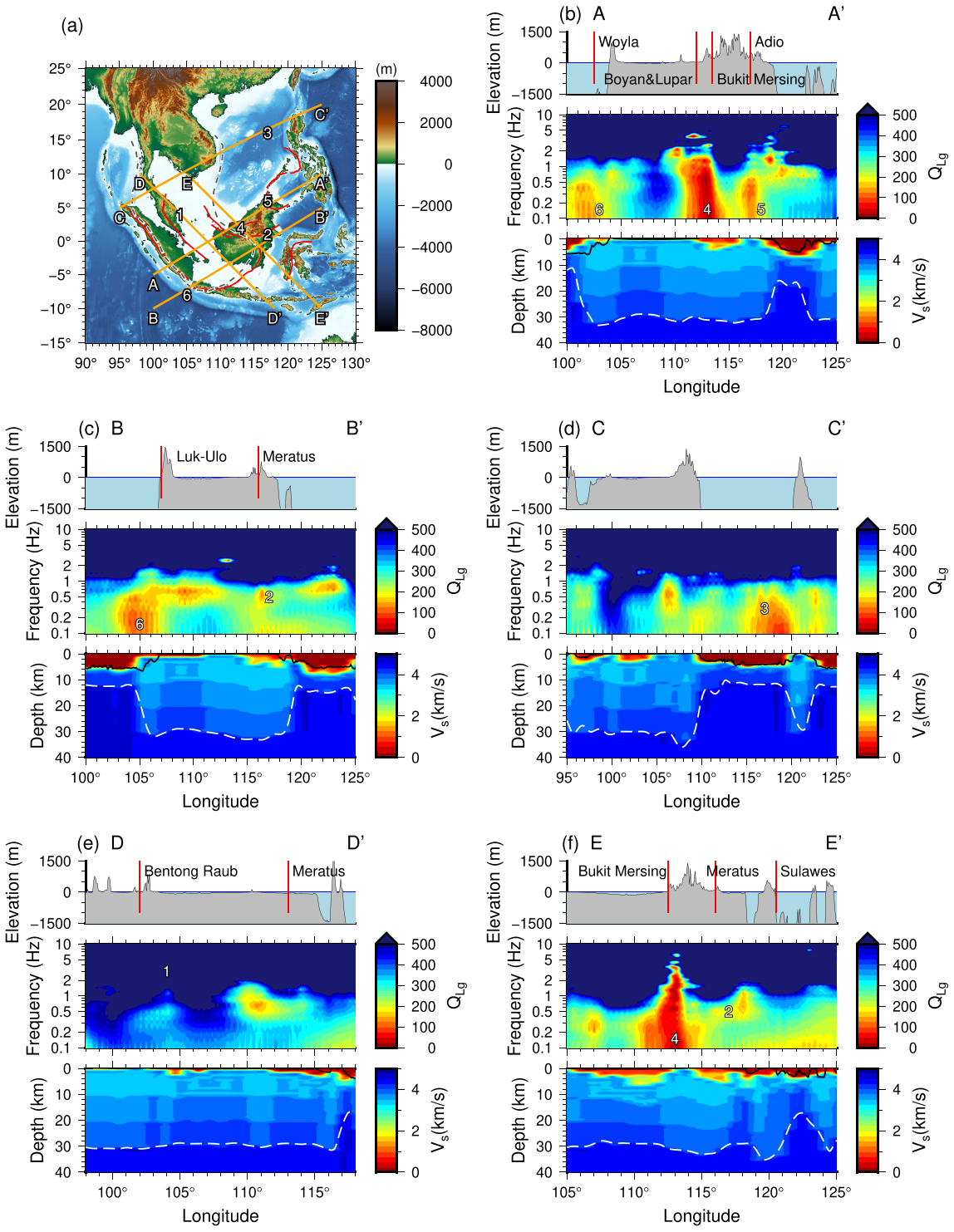

Figure 9. (a) Map showing the study region and locations of five cross-sections (yellow) which are displayed in (b)–(f). Each profile compares the surface topography (top panel), Q_{Lg} versus frequency (middle panel), and V_s profile from CRUST1.0 (Laske *et al.* 2013) (bottom panel). Major sutures are shown by red lines. In the lower panels, Moho discontinuities are shown in white dashed lines. The elevations in the upper panels are extracted from ETOPO1 model (Amante & Eakins 2009). Both the shear wave velocity and Moho depth are retrieved from CRUST1.0 (Laske *et al.* 2013).

Metcalfe (2017), we infer that the complete closure of northern Borneo occurring in Cenozoic contributed to the strong crustal attenuation in Sarawak. Although a study by Breitfeld *et al.* (2017) proposed that the accretion of Sarawak happened in Mesozoic, more evidences are necessary to determine the exact evolution history. The cause of the uplift in the Sarawak region may be due to the shortening of the crust caused by the rotation. The crust in the Borneo Core shows high-Q values, which indicates that the crust in these areas has remained stable and that the Borneo Core hardly deformed during its rotation.

5.5 Lg wave blockage

The Lg wave travels as a guided wave in the crust. When crossing the continental–oceanic boundary, due to the crust thinning, much of its energy escapes into the mantle within a short distance, and this is often referred to as the Lg-wave blockage. Several studies have observed Lg blockage at continental–oceanic transition zones, for example Sea of Japan (Hong 2010; Furumura *et al.* 2014; Xie & Zhao 2018) and northeast of Canada (Mousavi *et al.* 2014). Although it appears a simple process under the narrow-band observation and at long distance, the blockage is much complex under broad frequency band and looking at a close in range. The broad-band Lg-wave data set and variety of land–ocean transition types in Southeast Asia provide a unique example to investigate the blockage effect. In Figs 6 and 9, the oceanic basin in South China Sea is shown as a low-Q anomaly (coded #3). Regional waves crossing South China Sea in Figs 3 and 4 are depleted in Lg energy. The thinning of crust significantly reduces Lg energy, which is consistent with the simulation by Furumura *et al.* (2014). Only weak Lg waves can be observed at short distances and results in very low Q in this area. Similar phenomenon is observed in Figs 9(b) and (c), in which low-Q anomalies (coded #6) can be seen at lower frequencies near 101°E along Profile A and 104°E along Profile B, where the Indo–Australian Plate subducted eastward under the Eurasian Plate.

6 CONCLUSION

In this study, we investigated the regional Lg-wave attenuation in Southeast Asia. Using regional broad-band seismic records, we inverted regional Q_{Lg} models in a frequency band between 0.05 and 10.0 Hz. The results show good coverage and resolution in most parts of the study region, including Borneo, Malay Peninsula, Sumatra, Java and the surrounding continental shelves. The maps of spatial variations in Q_{Lg} values are consistent with the present day and historical tectonic activities in Southeast Asia. Our study demonstrated that inversion of the frequency-dependent Lg-wave Q model can be applied to regions composed of continents, islands and marginal seas, considerably expanding the range of applications of Lg-wave attenuation studies. Lg blockage is observed at the continental–oceanic transition zones in South China Sea and Indo–Australian subduction zone. The attenuation anomalies revealed in our Q_{Lg} models are consistent with the geological settings and the results from previous studies, providing new seismological constraints on the crustal structures and tectonic evolution in Southeast Asia.

Our Lg-wave Q models show that the prominent high-Q_{Lg} anomalies are located in regions with stable ancient crust, including the Malay Peninsula, East Sumatra, Sunda Shelf and Borneo Core. The result provides further evidence for the origin of Borneo, indicating that the Borneo Core is a firm part of the Sundaland Block and has remained stable during the regional tectonic evolution, including the rotation of Borneo and the accretion of surrounding terranes. Strong attenuation (low Q_{Lg}) is observed in regions with complex tectonic conditions, including sutures in Sabah, Sarawak, and the subduction zone of the Indo–Australian Plate under Eurasia. The collision of tectonic blocks results in strong attenuations, which provide significant constraints for investigating the block affinities.

Lateral variation of the Lg-wave attenuation in the crust relates to regional tectonic evolution in Southeast Asia. Typically, the Bentong-Raub line, formed during the closure of the Paleo-Tethys Ocean and the accretion of the Sundaland Core in Triassic, shows the highest Q_{Lg}. The Woyla, Meratus and Luk-Ulo sutures, related to the closure of the Meso-Tethys Ocean in the Cretaceous, show moderate attenuation. The Cenozoic collision between East and West Sulawesi and the subduction of the Proto-South China Sea in Sabah and Cagayan are associated with strong attenuation anomalies. Thus, alongside with other geological criteria, the links between crustal Q anomalies and tectonics can be useful for investigating regional tectonic evolution.

ACKNOWLEDGEMENTS

The authors thank Xi He, Lei Zhang, Lin Shen, Xiao Ma, Yi-Shan Song and Wei-Mou Zhu at the Institute of Geology and Geophysics, Chinese Academy of Sciences, and Xu Yang, Chen-Xu Chen, Qi-Hui Xu, Bo-Nan Cao, Yan-Zhao Yang, Jing Wang, Si-Yuan Zhang and Li Zhao at the Peking University, for engaging in discussions on this work. The constructive comments from the editor G. Laske, assistant editor L. Alexander and three reviewers, S. M. Mousavi, E. Sandvol and an anonymous one, greatly improved this paper and are appreciated. This research was supported by the National Natural Science Foundation of China (41630210, 41674060, 41974061 and 41974054) and the Special Fund of China Seismic Experimental Site (2019CSES0103 and 2016CESE0203). Seismic waveforms used in this study were retrieved with the software JWEEDv4.1r3 and downloaded from the Incorporated Research Institutions for Seismology (IRIS) Data Services (http://ds.iris.edu/ds/nodes/dmc/). Some figures were generated by the Generic Mapping Tools 6 (Wessel *et al.* 2019; https://www.generic-mapping-tools.org/).

REFERENCES

Advokaat, E., Marshall, N., li, S., Spakman, W., Krijgsman, W. & Hinsbergen, D., 2018. Cenozoic rotation history of Borneo and Sundaland, SE Asia revealed by paleomagnetism, seismic tomography, and kinematic reconstruction, *Tectonics,* **37,** 2486–2512.

Amante, C. & Eakins, B.W., 2009. ETOPO1 1 arc-minute global relief model: procedures, data sources and analysis, in *NOAA Technical Memorandum NESDIS NGDC-24,* National Geophysical Data Center, NOAA.

Bird, P., 2003. An updated digital model of plate boundaries, *Geochem. Geophys. Geosyst.,* **4,** doi:10.1029/2001GC000252.

Breitfeld, H.T., Hall, R., Galin, T., Forster, M.A. & BouDagher-Fadel, M.K., 2017. A Triassic to Cretaceous Sundaland–Pacific subduction margin in West Sarawak, Borneo, *Tectonophysics,* **694,** 35–56.

Chan, C.-H. *et al.*, 2017. Toward uniform probabilistic seismic hazard assessments for Southeast Asia, in *AGU Fall Meeting Abstracts*.

Chen, Y. & Xie, J., 2017. Resolution, uncertainty and data predictability of tomographic Lg attenuation models—application to Southeastern China, *Geophys. J. Int.,* **210,** 166–183.

Furumura, T., Hong, T.-K. & Kennett, B.L., 2014. Lg wave propagation in the area around Japan: observations and simulations, *Prog. Earth Planet. Sci.,* **1,** 10.

Global Volcanism Program, 2013. *Volcanoes of the World, v. 4.10.0 (14 May 2021)*. In: Venzke, E., (ed.). Smithsonian Institution.

Hall, R., 1996. Reconstructing Cenozoic SE Asia, in *Tectonic Evolution of Southeast Asia,* pp. 153–184, eds Hall, R. & Blundell, D., Geological Society Special Publication.

Hall, R., 2012. Late Jurassic–Cenozoic reconstructions of the Indonesian region and the Indian Ocean, *Tectonophysics,* **570–571,** 1–41.

Hall, R. & Breitfeld, T., 2017. Nature and demise of the Proto-South China Sea, *Bull. Geol. Soc. Malays.,* **63,** 61–76.

Hall, R. & Wilson, M.E.J., 2000. Neogene sutures in eastern Indonesia, *J. Asian Earth Sci.,* **18,** 781–808.

Herrmann, R.B. & Kijko, A., 1983. Short-period Lg magnitudes: instrument, attenuation, and source effects, *Bull. seism. Soc. Am.,* **73,** 1835–1850.

Hong, T.-K., 2010. Lg attenuation in a region with both continental and oceanic environments, *Bull. seism. Soc. Am.,* **100,** 851–858.

Honza, E. & Fujioka, K., 2004. Formation of arcs and backarc basins inferred from the tectonic evolution of Southeast Asia since the Late Cretaceous, *Tectonophysics,* **384,** 23–53.

Huang, Z., Zhao, D. & Wang, L., 2015. *P* wave tomography and anisotropy beneath Southeast Asia: insight into mantle dynamics, *J. geophys. Res.,* **120,** 5154–5174.

Hutchison, C.S., 1996. The 'Rajang accretionary prism' and 'Lupar Line' problem of Borneo, in *Tectonic Evolution of Southeast Asia,* pp. 247–261, eds. Hall, R. & Blundell, D., Geological Society Special Publication.

Laske, G., Masters, G., Ma, Z. & Pasyanos, M., 2013. Update on CRUST1.0—A 1-degree global model of Earth's crust, in *EGU General Assembly Conference*.

Lebedev, S. & Nolet, G., 2003. Upper mantle beneath Southeast Asia from *S* velocity tomography, *J. geophys. Res.,* **108,** doi:10.1029/2000JB000073.

Legendre, C.P., Zhao, L. & Chen, Q.F., 2015. Upper-mantle shear-wave structure under East and Southeast Asia from automated multimode inversion of waveforms, *Geophys. J. Int.,* **203,** 707–719.

Metcalfe, I., 2011. Tectonic framework and Phanerozoic evolution of Sundaland, *Gondwana Res.,* **19,** 3–21.

Metcalfe, I., 2017. Tectonic evolution of Sundaland, *Bull. Geol. Soc. Malays.,* **63,** 27–60.

Mitchell, B.J., Xie, J. & Lin, W., 1993. Attenuation of multiphase surface waves in the basin and range province Part II: the fundamental mode, *Seismol. Res. Lett.,* doi:10.1785/gssrl.64.3-4.239.

Mitchell, B.J., Pan, Y., Xie, J. & Cong, L., 1997. *Lg* coda *Q* variation across Eurasia and its relation to crustal evolution, *J. geophys. Res.,* **102,** 22767–22779.

Mousavi, S.M., Cramer, C.H. & Langston, C.A., 2014. Average Q_{Lg}, Q_{Sn}, and observation of Lg blockage in the Continental Margin of Nova Scotia, *J. geophys. Res.,* **119,** 7722–7744.

Müller, R.D., Sdrolias, M., Gaina, C. & Roest, W.R., 2008. Age, spreading rates, and spreading asymmetry of the world's ocean crust, *Geochem. Geophys. Geosyst.,* **9,** doi:10.1029/2007GC001743.

Paige, C.C. & Saunders, M.A., 1982. LSQR: an algorithm for sparse linear equations and sparse least squares, *ACM Trans. Math. Softw.,* **8,** 43–71.

Pasyanos, M.E., Matzel, E.M., Walter, W.R. & Rodgers, A.J., 2009. Broadband Lg attenuation modelling in the Middle East, *Geophys. J. Int.,* **177,** 1166–1176.

Phillips, W.S., Hartse, H.E. & Rutledge, J.T., 2005. Amplitude ratio tomography for regional phase Q, *Geophys. Res. Lett.,* **32,** doi:10.1029/2005GL023870.

Shi, X., Kirby, J., Yu, C., Jiménez-Díaz, A. & Zhao, J., 2017. Spatial variations in the effective elastic thickness of the lithosphere in Southeast Asia, *Gondwana Res.,* **42,** 49–62.

Simons, W.J.F. *et al.*, 2007. A decade of GPS in Southeast Asia: resolving Sundaland motion and boundaries, *J. geophys. Res.,* **112,** doi:10.1029/2005JB003868.

Street, R.L., Herrmann, R.B. & Nuttli, O.W., 1975. Spectral characteristics of the Lg wave generated by central United States earthquakes, *Geophys. J. Int.,* **41,** 51–63.

Wessel, P., Luis, J.F., Uieda, L., Scharroo, R., Wobbe, F., Smith, W.H.F. & Tian, D., 2019. The Generic Mapping Tools Version 6, *Geochem. Geophys. Geosyst.,* doi:10.1029/2019GC008515.

Xie, J., 1993. Simultaneous inversion for source spectrum and path *Q* using *Lg* with application to three Semipalatinsk explosions, *Bull. seism. Soc. Am.,* **83,** 1547–1562.

Xie, J. & Mitchell, B.J., 1990. Attenuation of multiphase surface waves in the Basin and Range province, part I *Lg* and *Lg* coda, *Geophys. J. Int.,* doi:10.1111/j.1365-246X.1990.tb00535.x.

Xie, J., Gok, R., Ni, J. & Aoki, Y., 2004. Lateral variations of crustal seismic attenuation along the INDEPTH profiles in Tibet from *Lg Q* inversion, *J. geophys. Res.,* **109,** doi:10.1029/2004JB002988.

Xie, X.B. & Zhao, L.F., 2018. The seismic characterization of North Korea underground nuclear tests (in Chinese with English abstract), *Chin. J. Geophys.,* **61,** 889–904.

Yan, J., 2005. Tectonic implications of marine mesozoic deposits from Kalimantan and Malay peninsula (in Chinese with English abstract), *J. Tropical Oceanogr.,* **24,** 26–32.

Yang, M. & Peng, S., 2004. Geodynamical features and geotectonic evolution of Kalimantan and adjacent areas, *J. Cent. South Univ. Technol.,* **11,** 312–315.

Yu, C., Shi, X., Yang, X., Zhao, J., Chen, M. & Tang, Q., 2017. Deep thermal structure of Southeast Asia constrained by *S*-velocity data, *Mar. Geophys. Res.,* **38,** 341–355.

Zahirovic, S., Seton, M. & Müller, R.D., 2014. The Cretaceous and Cenozoic tectonic evolution of Southeast Asia, *Solid Earth,* **5,** 227–273.

Zhang, T.-R. & Lay, T., 1995. Why the Lg phase does not traverse oceanic crust, *Bull. seism. Soc. Am.,* **85,** 1665–1678.

Zhao, L.F. & Xie, X.B., 2016. Strong Lg-wave attenuation in the Middle East continental collision orogenic belt, *Tectonophysics,* **674,** 135–146.

Zhao, L.F., Xie, X.B., Wang, W.M., Zhang, J.H. & Yao, Z.X., 2010. Seismic *Lg*-wave *Q* tomography in and around Northeast China, *J. geophys. Res.,* **115,** doi:10.1029/2009JB007157.

Zhao, L.F., Xie, X.B., He, J.K., Tian, X.B. & Yao, Z.X., 2013a. Crustal flow pattern beneath the Tibetan Plateau constrained by regional Lg-wave Q tomography, *Earth planet. Sci. Lett.,* **383,** 113–122.

Zhao, L.F., Xie, X.B., Wang, W.M., Zhang, J.H. & Yao, Z.X., 2013b. Crustal Lg attenuation within the North China Craton and its surrounding regions, *Geophys. J. Int.,* **195,** 513–531.

Zhao, L.F., Xie, X.B., Wang, W.M. & Yao, Z.X., 2018. A broadband crustal Lg wave attenuation model in Northeast China and the Korean Peninsula (in Chinese with English abstract), *Chin. J. Geophys.,* **61,** 856–871.

SUPPORTING INFORMATION

Supplementary data are available at *GJI* online.

Table S1. Codes and locations of the stations used in this study.
Table S2. Networks used in this study.
Table S3. Earthquake parameters used in this study.

Please note: Oxford University Press is not responsible for the content or functionality of any supporting materials supplied by the authors. Any queries (other than missing material) should be directed to the corresponding author for the paper.